

RESEARCH ARTICLE

Grain boundary energies in yttria-stabilized zirconia

Shen J. Dillon¹  | Yu-Feng Shen² | Gregory S. Rohrer³ 

¹ Department of Materials Science and Engineering, University of California, Irvine, California, USA

² Department of Physics, Carnegie Mellon University, Pittsburgh, Pennsylvania, USA

³ Department of Materials Science and Engineering, Carnegie Mellon University, Pittsburgh, Pennsylvania, USA

Correspondence

Gregory S. Rohrer, Department of Materials Science and Engineering, Carnegie Mellon University, Pittsburgh, PA 15213, USA.

Email: gr20@andrew.cmu.edu

Funding information

National Science Foundation, Grant/Award Number: DMR 1628994; Materials Characterization Facility at Carnegie Mellon University, Grant/Award Number: MCF-677785

Abstract

The three-dimensional microstructure of 8% yttria-stabilized zirconia (YSZ) was measured by electron backscatter diffraction and focused ion beam serial sectioning. The relative grain boundary energies as a function of all five crystallographic grain boundary parameters were determined based on the assumption of thermodynamic equilibrium at the internal triple junctions. Grain boundaries with (100) orientations have low energies compared to boundaries of other orientations, and all [100] twist boundaries have relatively low energies. Other classes of boundaries with lower than average energies include [100] symmetric tilt boundaries with disorientations less than 40° and [111] twist boundaries with disorientations greater than 20°. At fixed misorientations, the relative areas of boundaries are inversely correlated to the relative grain boundary energy. The results suggest that texturing microstructures to increase the relative areas of [100] twist boundaries might increase the oxygen ion conductivity of YSZ ceramics.

KEYWORDS

grain boundaries, microstructure, zirconia: yttria stabilized

1 | INTRODUCTION

Grain boundaries are important structural defects that can influence the electrical,¹ optical,² and mechanical³ properties of ceramics. For example, the transport of oxygen ions across grain boundaries in fast ion conducting yttria-stabilized zirconia (YSZ) is slower than conduction in the bulk lattice.^{4–7} As a result, grain boundaries increase the resistivity of YSZ ceramics used as solid electrolytes. It is expected that all grain boundaries in YSZ ceramics do not have the same ionic conductivity. The physical properties of grain boundaries are sensitive to their structure and crystallography, and, because grain boundaries have five crystallographic degrees of freedom, the number of structurally distinct grain boundaries is large.⁸ Assuming that some grain boundaries have lower ionic conductivities than others, one could hypothesize crystallographic textures that have increased conductivities compared to others. However, little is known about how the grain boundary properties of YSZ vary with crystallography.

The origin of the grain boundary resistance is thought to be the grain boundary space charge, which reduces the oxygen vacancy concentration in the vicinity of the boundary.^{9–11} The grain boundary space charge contributes to the grain boundary energy; thermodynamic assessments of this contribution indicate that grain boundaries with larger excess energies have larger space charges and, therefore, greater blocking potentials.^{12,13} According to this relationship, measurements of the grain boundary energy might provide guidance for the trends in the grain boundary blocking potential. Note that we are not proposing a strict correlation between energy and ionic conductivity for all boundaries, as one can imagine boundaries with special structures that block or promote oxide ion transport regardless of their space charge and grain boundary energy. However, in the most general case, a relationship between grain boundary energy and blocking potential makes sense because the lower the energy of the grain boundary, the more it resembles the high conductivity ideal lattice, and this results in a smaller space charge and reduced

blocking of oxygen ions. A small number of grain boundary energies have been measured^{14,15} and computed^{16,17} in the past. Fisher and Matsubara et al.¹⁶ reported that for a $\Sigma 5$ grain boundary ($\Sigma 5$ is coincident site lattice notation¹⁸ for a boundary with a 36° misorientation about the $[100]$ axis), the twist boundary had a lower energy and higher diffusivity than the $\Sigma 5$ symmetric tilt grain boundary, consistent with the proposed relationship between grain boundary energy and grain boundary conductivity.

While it would be challenging to measure the ionic conductivity of all types of grain boundaries, it is possible to measure relative grain boundary energies over all of the crystallographic parameters, and these energies might serve as relative indicators of the ionic conductivity of the boundary. Morawiec¹⁹ developed a method to determine the relative grain boundary energies of all types of grain boundaries using measurements of the geometry and crystallography of triple junctions and the assumption of local thermodynamic equilibrium at the junction. The method requires the characterization of many ($>10^4$) triple junctions, so three-dimensional (3D) orientation maps of polycrystals are required. The method has been applied to a number of materials,^{20–23} and, in one instance when the results were compared to simulation,²⁴ there was considerable agreement between the simulated and measured energies. The Morawiec method has recently been improved, mainly by eliminating the need to discretize the five-parameter space of grain boundary types, and this new method will be applied here to YSZ.²⁵

The purpose of this paper is to report on the relative grain boundary energies of YSZ. The microstructure of a YSZ ceramic was mapped by 3D electron backscatter diffraction (EBSD) using a dual beam-focused ion beam (DB-FIB) scanning electron microscope (SEM). From a microstructure containing more than 4×10^3 grains, more than 8×10^4 triple junctions were characterized. While the distribution of grain boundary areas and energies were relatively isotropic compared to some other materials, (100) twist boundaries were found to have greater relative areas and lower relative energies. This finding has implications for the design of microstructures with improved ionic conductivities.

2 | EXPERIMENTAL METHODS

The YSZ ceramics with the cubic fluorite crystal structure ($Fm\bar{3}m$) were prepared by sintering commercially obtained powders with a 300–500 nm particle size (Nex-Tech Materials, Lewis Center, OH) at 1450°C for 4 h in air, as described previously.²⁶ Plate-shaped samples were then cut to less than 1 mm thickness and polished to a final thickness in the range of 20–60 μm . The thin samples

were then broken, which creates triangular shards. After sputter-coating a triangular piece with ≈ 2 nm of Pt to prevent charging during the measurement, it was attached to a 45° SEM pre-tilt stub, exposing the sharp point of a triangle for the DB-FIB serial sectioning. This geometry allows material to be milled away without redeposition, eliminates problems associated with shadowing, and allows the sample to be tilted to 7° – 52° toward the ion-column for ion-milling or tilted 25° – 70° toward the EBSD detector for orientation mapping. Samples were ion milled at 30 kV and 7 nA using a Ga^+ ion beam. EBSD data were acquired at 20 kV and 9.5 nA, and orientations were measured on a square grid with a spacing of 200 nm in the X and Y directions; layers were separated by 400 nm. Two volumes of data were collected. The first was approximately $67 \times 70 \times 32 \mu\text{m}$, and the second was $90 \times 92 \times 27 \mu\text{m}$. Additional details of the data are described in the Supporting Information. The data and programs used to process the data can be downloaded from the Grain Boundary Data Archive.²⁷

The steps for processing the EBSD data and determining the grain boundary energy have been described in detail in earlier publications.^{20,21} Briefly, the analysis begins by identifying triple points on all parallel layers. Based on the similarity of grain orientations, triple points on adjacent layers that belong to the same triple line in the 3D structure are identified. Triple junctions are then parameterized by three tangent lines fit to the boundaries that meet on the first layer, three tangent lines fit to the boundaries that meet on the second layer, and the line connecting the two triple points. Grain boundary plane orientations are determined from the cross product of each tangent vector and the triple line vector. In all, 87 518 triple junctions were identified. Using these data, we determine the relative energy for each boundary under the assumptions that the Herring²⁸ condition for local interfacial equilibrium is obeyed at each junction and that grain boundaries close in crystallographic space have similar energies. The resulting relative energy distribution is normalized so that the average is 1. This is described completely in reference.²⁵ Simulations of the energy reconstruction process using a similar number of junctions and experimental uncertainties in the measured boundary orientation lead to the conclusion that the uncertainty of the energies is less than 0.03 relative units, and this uncertainty applies to all of the energies reported here.²⁵

The grain boundary character distribution, which is the relative areas of grain boundaries as a function of their five crystallographic parameters, was determined using a 3D reconstruction of the microstructure carried out in Dream.3D.²⁹ The pipelines used for the reconstruction are similar to the tutorial pipelines supplied with Dream.3D. The exact pipelines, and the resulting Dream.3D files used in this work, are available for download.²⁷ The

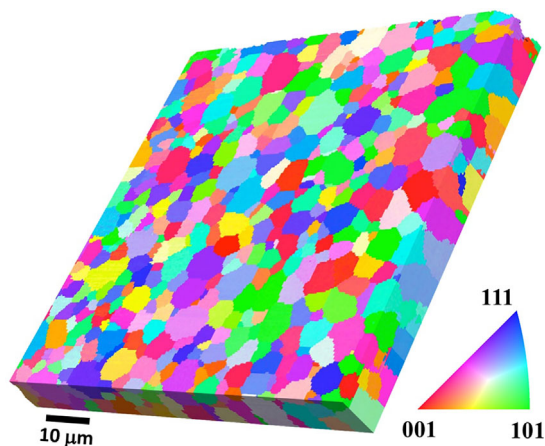


FIGURE 1 Example of the microstructure of 8% yttria-stabilized zirconia. The volume is $90\ \mu\text{m} \times 92\ \mu\text{m} \times 9.2\ \mu\text{m}$. The grains are colored by orientation, according to the color key in the lower right corner

reconstructed microstructure contained more than 4.2×10^3 grains with more than 2.5×10^4 grain faces. The spherical equivalent mean grain radius (standard deviation) is $2.02\ (0.95)\ \mu\text{m}$. This value is almost certainly an underestimate of the true average grain radius; the grains at the limits of the field of view in the 3D volume have sizes larger than measured, and this leads to the underestimation. In the reconstructed microstructure, the grain boundaries are represented by a mesh of triangles. For each of the more than 2.8×10^6 triangles in the mesh, we know the area, the normal direction, and the crystal orientation on both sides. This information specifies all five macroscopic grain boundary parameters. Similarly, for each triple line, we know the energy and the five macroscopic parameters for each boundary in the junction. The average relative grain boundary energy and area at any specific point in the five-parameter space are computed from these data using the kernel density approximation method.³⁰ For any given point in the five-dimensional (5D) space, the areas or energies of all boundary triangles within a 6° misorientation aperture and a 7° grain boundary plane inclination aperture are averaged.

3 | RESULTS

A section of the 3D microstructure, prior to meshing and smoothing of the interfaces, is illustrated in Figure 1. The microstructure has no significant texture, the grains are equiaxed, and the distribution of grain sizes does not show any grains that are more than three times the mean radius. The distribution of grain boundary disorientations (Figure S1) is very near the random distribution. The dis-

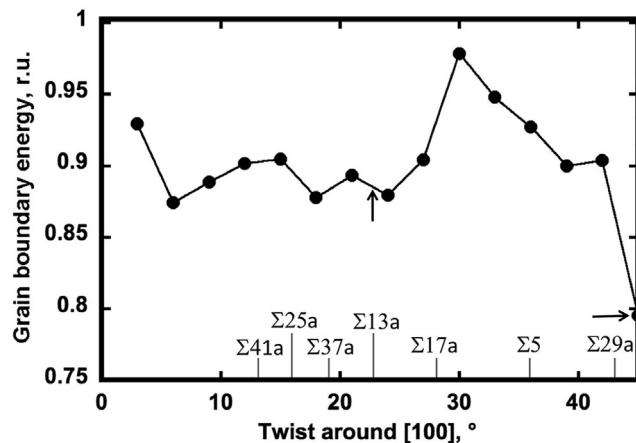


FIGURE 2 The grain boundary energies of [100] twist boundaries in yttria-stabilized zirconia (YSZ), sampled at 3° intervals. As reference points, coincident site lattice disorientations with $\Sigma \leq 49$ are marked along the lower axis. The arrows mark the positions of the disorientations used in Figure 3 to illustrate the dependence of the grain boundary energy on the grain boundary plane orientation

tribution of grain boundary planes, irrespective of misorientation, shows relatively weak anisotropy, with the relative areas of (100) planes being larger than those with orientations near (110) or (111) (Figure S2A). The relative grain boundary energies are also nearly isotropic when projected in the crystal reference frame, with the energy of boundaries with the (100) orientation being slightly lower than (110) or (111) (Figure S2B). These results are consistent with previously reported grain boundary plane^{26,31} and energy²⁶ distributions in the 2D crystal reference frame. The isotropic nature of the grain boundary plane distribution in the 2D crystal reference frame is consistent with that measured for another fluorite structured ceramic, Ca-doped CeO_2 .³²

The anisotropy of the grain boundary energy is more significant when one examines the variations in the 5D space of grain boundary types. For example, Figure 2 shows the grain boundary energies of (100) twist grain boundaries. All of these energies are less than the average grain boundary energy (1.0). By definition, the twist boundaries have (100) planes on both sides of the boundary. The grain boundary relative energy as a function of grain boundary inclination is illustrated at two fixed [100] disorientations ($22.6^\circ/[100]$ [$\Sigma 13a$] and $45^\circ/[100]$ [$\Sigma 169$]) in Figure 3. Both grain boundary energy distributions have a minimum at the (100) orientation of the twist grain boundary. These two examples are representative of all the [100] disorientations. The grain boundary area distributions (Figure S3) have maxima at these positions, consistent with previously reported stereologically measured area distributions.³³

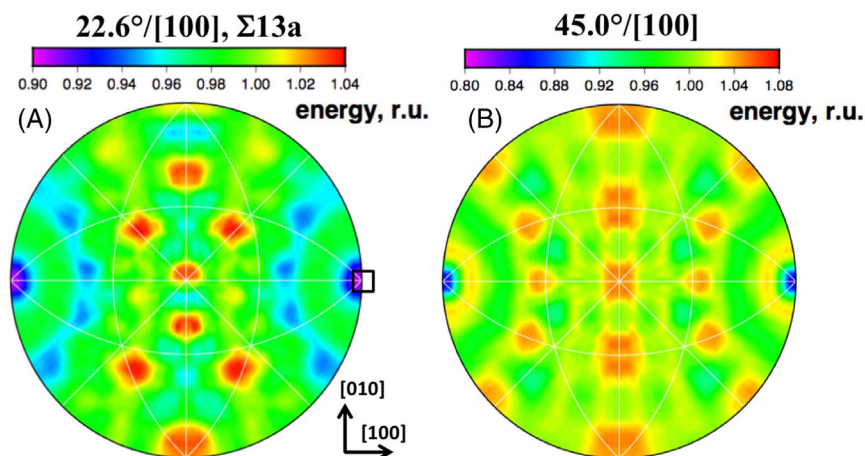


FIGURE 3 Grain boundary energy distributions for the 22.6°/[100] (A) and the 45°/[100] (B) disorientations. The distributions are plotted on stereographic projections along the [001] direction; the orientation of the in plane vectors is shown in (A). The [100] disorientation axis is denoted by the black square in (A)

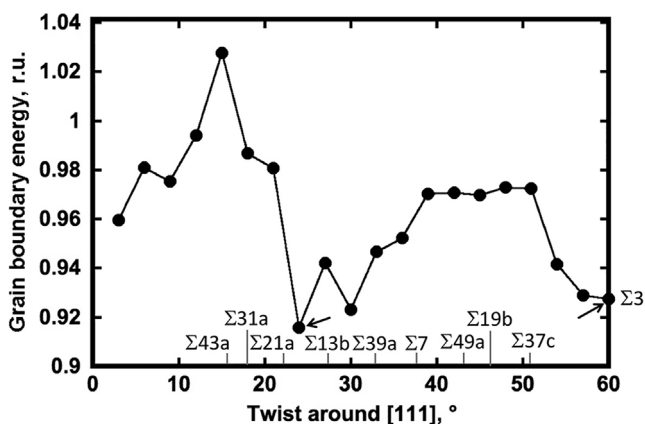


FIGURE 4 The grain boundary energies of [111] twist boundaries in yttria-stabilized zirconia (YSZ), sampled at 3° intervals. As reference points, coincident site lattice disorientations with $\Sigma \leq 49$ are marked along the lower axis. The arrows mark the positions of the disorientations used in Figure 5 to illustrate the dependence of the grain boundary energy on the grain boundary plane orientation

When the variations in the energy of twist boundaries with rotations about [111] are examined (Figure 4), it is found that boundaries with disorientations greater than 20° have lower than average energies. While this is a similar to the observations for [001] twist boundaries, the [111] twist boundary energies are not as low. Because local minima are found at 24°/[111] ($\Sigma 67$) and 60°/[111] ($\Sigma 3$), the variations of the grain boundary energy as a function of grain boundary plane inclination are illustrated in Figure 5. For both cases, the grain boundary relative energy has a minimum at the twist position (the (111) orientation). The grain boundary area distribution for the $\Sigma 3$ (Figure S4B) disorientation has a maximum at the (111) orientation, consistent with stereologically measured area distribution.³³ A survey of the energies of other symmetric tilt and twist grain boundaries for other low index axes is presented in Figure S5.

When the data in Figure 3 are compared to the data in Figure S3, it is clear that lowest energy boundary orientations usually have the highest relative area. This suggests that the relative grain boundary area is inversely correlated to the grain boundary energy, and this is true for many fixed misorientations. For example, Figure 6 illustrates the correlation between the energy and relative area for two boundaries. In agreement with expectations from previous studies of other polycrystals,³⁴ there are more low energy grain boundaries and fewer high energy grain boundaries. While stronger correlations are usually found in materials with strongly anisotropic distributions,²² the results in Figure 6 are consistent with grain boundary energy-area correlations in more isotropic materials.²⁰

4 | DISCUSSION

As expected, there is no apparent correlation between the grain boundary energy and the inverse coincidence (Σ) number. While it is true that there is a local minimum at the $\Sigma 3(111)$ twist boundary (Figures 4 and 5B), there are other minima with lower energies at higher values of Σ , such as the twist boundary in Figure 3B, which is approximately $\Sigma 167$. The fact that the energy is not related to Σ is consistent previous studies³⁴ and computational surveys of grain boundary energies.^{35,36} Instead, low grain boundary energies in oxide ceramics are often associated with low index grain boundary planes. Here, grain boundary planes with the (100) orientation are low energy, as was found for rock salt structured MgO²² and perovskite structured SrTiO₃.²³ The observation of low energy [100] twist boundaries is consistent with the idea that the (100) orientation represents a minimum in the energy. Also consistent with the previous studies, there is an inverse correlation between the energy and relative areas of grain boundaries (Figure 6).

FIGURE 5 Grain boundary energy distributions for the (A) $24^\circ/[111]$ and the (B) $60^\circ/[111]$ disorientations. The distributions are plotted on stereographic projections along the $[001]$ direction; the orientation of the in plane vectors is shown in (A). The $[111]$ disorientation axis is denoted by the white triangle in (A)

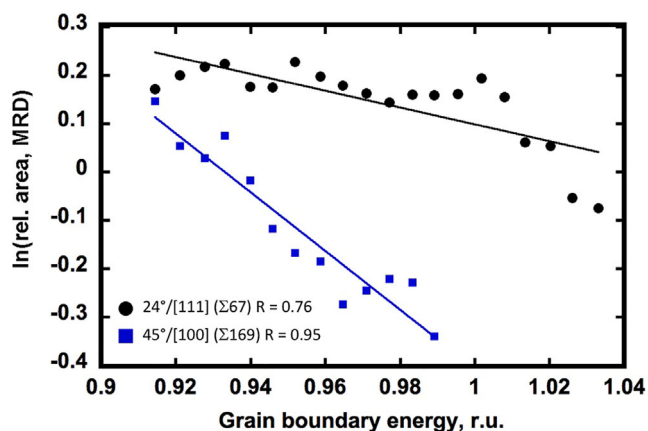
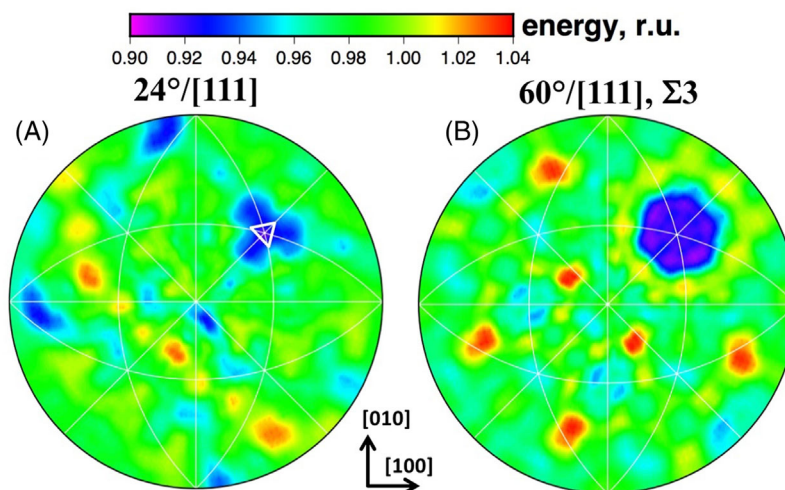


FIGURE 6 Correlations between the grain boundary energy and area for grain boundaries with the $24^\circ/[111]$ (black circles) and $45^\circ/[100]$ (blue squares). The best fit lines are superposed on the data. The relative area is in units of multiples of a random distribution (MRD)

The systematically low energies of the $[100]$ twist boundaries in YSZ suggest a structural origin for this phenomenon. While the grain boundaries of YSZ have been extensively studied by high-resolution transmission electron microscopy (HRTEM),^{14,15,37–39} there is a complete absence of data on $[100]$ twist grain boundaries and twist boundaries in general. This is because of a limitation of HRTEM; to resolve atomic columns in both crystals on either side of the boundary, they must share a common zone axis, and this condition is only met for tilt grain boundaries when looking along the plane of the boundary. Calculations of YSZ grain boundary energies have also focused on tilt boundaries, except for the study of Fisher and Matsubara et al.¹⁶ who compared the energy of a $\Sigma 5$ tilt and twist grain boundary and found that the twist boundary had a lower energy, consistent with present findings.

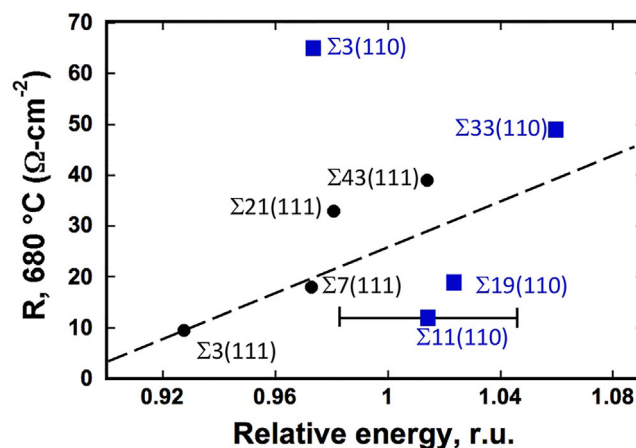


FIGURE 7 Comparison of measured resistance of twist boundaries in yttria-stabilized zirconia (YSZ) reported by Ye et al.⁴¹ and grain boundary energies from the present study. The horizontal bar through the point for $\Sigma 11(110)$ illustrates an uncertainty estimate (± 0.03) for each energy value. The dashed line is a linear fit to seven points (excluding $\Sigma 3(110)$) with a correlation coefficient of 0.65

There have been some studies of grain boundary conductivities of YSZ bicrystals.^{5,40,41} Ye et al.⁴¹ measured the resistances of four $[111]$ and $[110]$ twist grain boundaries in YSZ bicrystals, and these results are compared to the measured grain boundary energies in Figure 7. For the series of $[111]$ twist boundaries, the relative grain boundary energy and resistivity show a positive correlation. For the series of $[110]$ twist boundaries, three of the four show a positive correlation between energy and resistance. The outlier in this trend is the $\Sigma 3(110)$ boundary; its measured energy is below average, but it had the highest measured resistance. If we ignore this boundary, a linear fit to the other seven data points (the dashed line in Figure 7) shows a positive correlation with a correlation coefficient of 0.65. While it is difficult to draw definitive conclusions from eight

data points, Figure 7 provides some support for that idea that lower energy grain boundaries on average have lower resistances.

While there are no conductivity data for bicrystals with [100] misorientations, Kiguchi et al.⁴² reported that the ionic conductivity of columnar YSZ films increased with the strength of the [100] texture. The most strongly textured film had an ionic conductivity 30 times greater than that of a film with no texture and a higher density of grain boundaries. In a columnar microstructure, stronger [100] texture will increase the fraction of boundaries with [100] misorientations, and these are boundaries with lower than average energies. If the low relative grain boundary energy of boundaries with [100] misorientations is the reason for the higher ionic conductivity, then the ideal microstructure would have biaxial texture with the majority of the grain boundaries having low misorientation angles about [100]. Based on Figure 2 and Figure S5A, twist and symmetric tilt boundaries with misorientations $<20^\circ$ have systematically lower energies.

The finding that certain classes of grain boundaries (such as [100] twists) have lower relative energy and that minima are found in places that are not predictable based on symmetry considerations (such as $24^\circ/(111)$) illustrates the advantage of using 3D microstructure data to measure properties in the 5D space of grain boundary parameters. Because all possibilities are examined, there is no selection bias in the individual boundaries examined. For example, an earlier study evaluated the energies of a set of symmetric tilt grain boundaries with low Σ values using measurements of grain boundary thermal grooves,^{14,15} but this set did not include the lowest energy boundaries identified here. Furthermore, by identifying the classes of low energy boundary types (for example, [100] twist boundaries) rather than particular boundaries with low energy, it is possible to propose textures that might exhibit lower grain boundary resistance.

5 | CONCLUSIONS

The relative energies of grain boundaries in a YSZ ceramic have been determined from the geometry of the triple junctions. The energies are specified throughout the five-parameter domain of crystallographic parameters. Grain boundaries with (100) orientations have low energies compared to boundaries of other orientations. All [100] twist boundaries have relatively low energies, and [100] symmetric tilt boundaries with misorientations less than 40° and [111] twist boundaries with disorientations greater than 20° have lower than average energies. Assuming that low energy grain boundaries have higher transverse ionic conductivity, then YSZ ceramics with [100] biaxial texture


should have greater oxygen ion conductivities than random microstructures.

ACKNOWLEDGMENTS

This work was supported by the National Science Foundation under grant DMR 1628994. The authors acknowledge the use of the Materials Characterization Facility at Carnegie Mellon University supported by grant MCF-677785 and Lam Helmick for providing the YSZ sample and Paul Salvador and Robert Suter for detailed comments on the manuscript.

ORCID

Shen J. Dillon  <https://orcid.org/0000-0002-6192-4026>

Gregory S. Rohrer  <https://orcid.org/0000-0002-9671-3034>

REFERENCES

- Dimos D, Chaudhari P, Mannhart J. Superconducting transport properties of grain-boundaries in $\text{YBa}_2\text{Cu}_3\text{O}_7$ bicrystals. *Phys Rev B*. 1990;41(7):4038–49.
- Apetz R, van Bruggen MPB. Transparent alumina: a light-scattering model. *J Am Ceram Soc*. 2003;86(3):480–6.
- Feng L, Hao R, Lambros J, Dillon SJ. The influence of dopants and complexion transitions on grain boundary fracture in alumina. *Acta Mater*. 2018;142:121–30.
- De Souza RA, Pietrowski MJ, Anselmi-Tamburini U, Kim S, Munir ZA, Martin M. Oxygen diffusion in nanocrystalline yttria-stabilized zirconia: the effect of grain boundaries. *Phys Chem Chem Phys*. 2008;10(15):2067–72.
- Nakagawa T, Sakaguchi I, Shibata N, Matsunaga K, Yamamoto T, Haneda H, et al. Oxygen diffusion blocking of single grain boundary in yttria-doped zirconia bicrystals. *J Mater Sci*. 2005;40(12):3185–90.
- Peters C, Weber A, Butz B, Gerthsen D, Ivers-Tiffée E. Grain-size effects in YSZ thin-film electrolytes. *J Am Ceram Soc*. 2009;92(9):2017–24.
- Verkerk MJ, Middelhuis BJ, Burggraaf AJ. Effect of grain-boundaries on the conductivity of high-purity $\text{ZrO}_2\text{-Y}_2\text{O}_3$ ceramics. *Solid State Ion*. 1982;6(2):159–70.
- Rohrer GS. Grain boundary energy anisotropy: a review. *J Mater Sci*. 2011;46(18):5881–95.
- Guo X, Maier J. Grain boundary blocking effect in zirconia: a Schottky barrier analysis. *J Electrochem Soc*. 2001;148(3):E121–E6.
- Guo X, Zhang ZL. Grain size dependent grain boundary defect structure: case of doped zirconia. *Acta Mater*. 2003;51(9):2539–47.
- Lee JS, Anselmi-Tamburini U, Munir ZA, Kim S. Direct evidence of electron accumulation in the grain boundary of yttria-doped nanocrystalline zirconia ceramics. *Electrochem Solid-State Lett*. 2006;9(8):J34–J6.
- De Souza RA, Dickey EC. The effect of space-charge formation on the grain-boundary energy of an ionic solid. *Philos Trans A Math Phys Eng Sci*. 2019;377(2152):20180430.

13. Vikrant KSN, Garcia RE. Charged grain boundary transitions in ionic ceramics for energy applications. *npj Comput Mater*. 2019;5. <https://doi.org/10.1038/s41524-019-0159-2>
14. Shibata N, Oba F, Yamamoto T, Ikuhara Y. Structure, energy and solute segregation behaviour of 110 symmetric tilt grain boundaries in yttria-stabilized cubic zirconia. *Philos Mag*. 2004;84(23):2381–415.
15. Yoshida H, Yokoyama K, Shibata N, Ikuhara Y, Sakuma T. High-temperature grain boundary and grain boundary energy in cubic sliding behavior zirconia bicrystals. *Acta Mater*. 2004;52(8):2349–57.
16. Fisher CAJ, Matsubara H. The influence of grain boundary misorientation on ionic conductivity in YSZ. *J Eur Ceram Soc*. 1999;19(6-7):703–7.
17. Gonzalez-Romero RL, Melendez JJ, Gomez-Garcia D, Cumbra FL, Dominguez-Rodriguez A. A molecular dynamics study of grain boundaries in YSZ: structure, energetics and diffusion of oxygen. *Solid State Ion*. 2012;219:1–10.
18. Adams BL, Zhao J, Grimmer H. Discussion of the representation of intercrystalline misorientation in cubic materials. *Acta Cryst A*. 1990;46:620–2.
19. Morawiec A. Method to calculate the grain boundary energy distribution over the space of macroscopic boundary parameters from the geometry of triple junctions. *Acta Mater*. 2000;48(13):3525–32.
20. Dillon SJ, Rohrer GS. Characterization of the grain-boundary character and energy distributions of yttria using automated serial sectioning and EBSD in the FIB. *J Am Ceram Soc*. 2009;92(7):1580–5.
21. Li J, Dillon SJ, Rohrer GS. Relative grain boundary area and energy distributions in nickel. *Acta Mater*. 2009;57(14):4304–11.
22. Saylor DM, Morawiec A, Rohrer GS. Distribution and energies of grain boundaries in magnesia as a function of five degrees of freedom. *J Am Ceram Soc*. 2002;85(12):3081–3.
23. Zhong XT, Kelly MN, Miller HM, Dillon SJ, Rohrer GS. Grain boundary curvatures in polycrystalline SrTiO₃: dependence on grain size, topology, and crystallography. *J Amer Ceram Soc*. 2019;102(11):7003–14.
24. Rohrer GS, Holm EA, Rollett AD, Foiles SM, Li J, Olmsted DL. Comparing calculated and measured grain boundary energies in nickel. *Acta Mater*. 2010;58(15):5063–9.
25. Shen YF, Zhong XT, Liu H, Suter RM, Morawiec A, Rohrer GS. Determining grain boundary energies from triple junction geometries without discretizing the five-parameter space. *Acta Mater*. 2019;166:126–34.
26. Helmick L, Dillon SJ, Gerdes K, Gemmen R, Rohrer GS, Seetharaman S, et al. Crystallographic characteristics of grain boundaries in dense yttria-stabilized zirconia. *Int J Appl Ceram Technol*. 2011;8(5):1218–28.
27. Rohrer GS Grain boundary data archive 2015. Available from: http://mimp.materials.cmu.edu/~gr20/Grain_Boundary_Data_Archive/YSZ_energy/YSZ_energy.html. Accessed date 17 December 2021.
28. Herring C. Surface tension as a motivation for sintering. In: Kingston WE, editor. *The physics of powder metallurgy*. New York: McGraw-Hill; 1951. p. 36.
29. Groeber MA, Jackson MA. DREAM.3D: a digital representation environment for the analysis of Microstructure in 3D. *Integr Mater Manuf Innovation*. 2014;3:56.
30. Glowinski K, Morawiec A. Analysis of experimental grain boundary distributions based on boundary-space metrics. *Metall Mater Trans A*. 2014;45A(8):3189–94.
31. Bobrowski P, Faryna M, Glowinski K. Evaluation of grain boundary plane distribution in yttria stabilized polycrystalline zirconia based on 3D EBSD analysis. *Mater Charact*. 2016;122:137–41.
32. Bowman WJ, Kelly MN, Rohrer GS, Hernandez CA, Crozier PA. Enhanced ionic conductivity in electroceramics by nanoscale enrichment of grain boundaries with high solute concentration. *Nanoscale* 2017;9(44):17293–302.
33. Kini MK. Grain boundary crystallography in polycrystalline yttria-stabilised cubic zirconia. *Philos Mag*. 2018;98(20):1865–83.
34. Rohrer GS. Measuring and interpreting the structure of grain-boundary networks. *J Am Ceram Soc*. 2011;94(3):633–46.
35. Olmsted DL, Foiles SM, Holm EA. Survey of computed grain boundary properties in face-centered cubic metals: I. Grain boundary energy. *Acta Mater*. 2009;57(13):3694–703.
36. Ratanaphan S, Olmsted DL, Bulatov VV, Holm EA, Rollett AD, Rohrer GS. Grain boundary energies in body-centered cubic metals. *Acta Mater*. 2015;88:346–54.
37. An J, Park JS, Koh AL, Lee HB, Jung HJ, Schoonman J, et al. Atomic scale verification of oxide-ion vacancy distribution near a single grain boundary in YSZ. *Sci Rep*. 2013;3:2680.
38. Dickey EC, Fan XD, Pennycook SJ. Structure and chemistry of yttria-stabilized cubic-zirconia symmetric tilt grain boundaries. *J Am Ceram Soc*. 2001;84(6):1361–8.
39. Feng B, Lugg NR, Kumamoto A, Ikuhara Y, Shibata N. Direct observation of oxygen vacancy distribution across yttria-stabilized zirconia grain boundaries. *ACS Nano*. 2017;11(11):11376–82.
40. Park JS, Kim YB, An J, Prinz FB. Oxygen diffusion across the grain boundary in bicrystal yttria stabilized zirconia. *Solid State Commun*. 2012;152(24):2169–71.
41. Ye F, Yin CY, Ou DR, Mori T. Relationship between lattice mismatch and ionic conduction of grain boundary in YSZ. *Prog Nat Sci Mater Int*. 2014;24(1):83–6.
42. Kiguchi T, Konno TJ, Funakubo H, Sakurai O, Shinozaki K. Columnar grain boundary coherence in yttria-stabilized zirconia thin film: effects on ionic conductivity. *J Ceram Soc Japan*. 2014;122(1421):72–7.

SUPPORTING INFORMATION

Additional supporting information may be found in the online version of the article at the publisher's website.

How to cite this article: Dillon SJ, Shen Y-F, Rohrer GS. Grain boundary energies in yttria-stabilized zirconia. *J Am Ceram Soc*. 2022;105:2925–2931. <https://doi.org/10.1111/jace.18283>